

Low-emittance tuning at the Cornell Electron Storage Ring Test Accelerator

J. Shanks,* D.L. Rubin, and D. Sagan
CLASSE, Cornell University, Ithaca, New York 14853, USA
(Dated: October 28, 2018)

In 2008 the Cornell Electron/Positron Storage Ring (CESR) was reconfigured from an electron/positron collider to serve as a testbed for the International Linear Collider (ILC) damping rings. One of the primary goals of the CESR Test Accelerator (CesrTA) project is to develop low emittance tuning techniques to achieve sub-10 pm geometric vertical emittance at 2.085 GeV. This paper discusses the tuning methods used at CesrTA to achieve low-emittance conditions. A minimum vertical emittance of $8.7 (+2.9/-3.4)^{sys} (\pm 0.2)^{stat}$ pm has been achieved at 2.085 GeV. In various configurations and beam energies the correction technique routinely achieves $\epsilon_y < 15$ pm after correction. Beam-based measurement and correction requires about 15 minutes. Simulations modeling the effects of magnet misalignments, BPM errors, and emittance correction algorithm suggest the residual vertical emittance measured at the conclusion of the tuning procedure is dominated by sources other than optics errors and misalignments.

I. INTRODUCTION

The Cornell Electron/Positron Storage Ring (CESR) is a 768 m storage ring with an energy reach of 1.5-5.3 GeV. CESR parameters are shown in Table I.

TABLE I. Parameters of the CESR electron/positron storage ring.

Parameter	Value	Units
Circumference	768.4	[m]
Energy	2.085 (1.5-5.3)	[GeV]
Lattice Type	FODO	
Symmetry	\approx Mirror	
H / V Steerings	55/58	
Quadrupoles	105	
Skew Quadrupoles	27	
Damping Wigglers	12	
Wiggler B_{max}	1.9	[T]
Position Monitors	100	
$\epsilon_x^{geometric}$	2.7	[nm]
$\epsilon_y^{geometric}$ (target)	10	[pm]

In 2008 CESR was reconfigured from an electron/positron collider to the CESR Test Accelerator (CesrTA) [1–3], a testbed for the International Linear Collider (ILC) damping rings. One of the primary goals of the CesrTA project has been to explore the efficacy of low-emittance tuning (LET) techniques being developed for the ILC damping rings.

In CESR, all quadrupoles, sextupoles, steering correctors and skew quadrupoles are independently powered. Combined with the broad energy reach and complete lack of low-order symmetry, CESR’s optics allow for significant flexibility. This capability is heavily utilized in CesrTA, where the experimental program requires perhaps a dozen different combinations of machine energies and optics during each 3-week period of dedicated

CesrTA machine studies. During these extensive studies periods conditions frequently change three or more times every day, as different groups have different optics requirements. To minimize the amount of time devoted to emittance tuning, the tuning algorithm is required to be fast, of order 10 minutes for one iteration, and conditions achieved after tuning must be reproducible.

This paper describes the optics correction procedure developed at CesrTA that meets these requirements and presents experimental results. Also discussed are simulations of the correction procedure, which have been essential to understanding measurement systematics and recognizing that the residual vertical emittance is dominated by sources other than optics errors and misalignments. In particular, noise from the transverse feedback amplifiers was found to increase the vertical emittance by 70%. The current and energy dependence of the emittance are also discussed.

II. MOTIVATION FOR EMITTANCE TUNING

Modern storage rings for x-ray light sources and damping rings for lepton colliders demand ultra-low emittance. The primary static contributions to vertical emittance in a planar ring are tilted and vertically-offset quadrupoles, and rolled dipoles. Tilted quadrupoles couple horizontal and vertical motion leading to an increase in b -mode (vertical mode) emittance. Vertical quadrupole offsets and dipole rolls introduce vertical kicks, generating vertical dispersion and thus vertical emittance. Additional sources of vertical emittance include time-dependent variations associated with line voltage, ground motion, and feedback systems, which contribute kicks to the beam in various ways, and current-dependent effects such as intra-beam scattering (IBS).

Without beam-based corrections of dispersion and coupling, the vertical emittance would be limited by the quality of survey and alignment. The measured distributions of surveyed quadrupole and dipole offsets and tilts for CESR are shown in Fig. 1. The root mean square

* js583@cornell.edu

(RMS) of the position and tilt measurements are summarized in Table IX, and include an estimated $100\ \mu\text{m}$ uncertainty in the displacement of the magnetic center from physical center of the magnet.

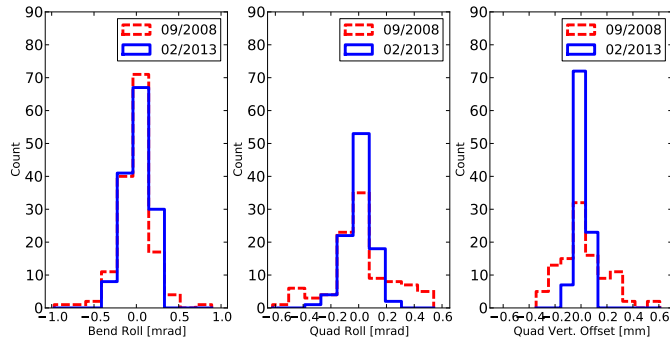


FIG. 1. Survey and alignment results for CesrTA as of December 2012 CesrTA run, compared to alignment in September 2008 at the start of the CesrTA program. Left to right: dipole roll, quadrupole tilt, and quadrupole vertical offset.

Simulations using random distributions of magnet errors consistent with the measured alignments summarized in Table IX, along with systematic and random multipoles summarized in Table X, have been used to study the effect of these errors on the vertical emittance. Repeating for 100 random sets of magnet errors, the resulting distributions of emittance, dispersion, and coupling yield statistical information about the probability of achieving the target emittance, and are shown in Fig. 2.

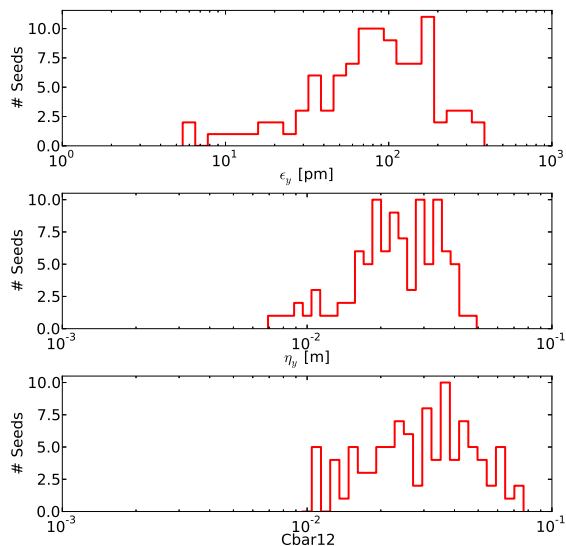


FIG. 2. Resulting distributions of vertical emittance, vertical dispersion, and coupling when applying random distributions of errors at the amplitudes specified in Table IX, along with systematic and random multipoles specified in Table X.

Without any beam-based corrections, simulations

show that out of 100 random seeds, only three yielded the target vertical emittance of $10\ \text{pm}$; the mean vertical emittance of the 100 seeds is $104\ \text{pm}$. It is evident that the survey and alignment techniques used are insufficient by themselves to reach the CesrTA emittance target. Some form of beam-based correction is clearly required in order to achieve and maintain low-emittance operating conditions.

III. MEASUREMENT TECHNIQUES

Beam position monitors (BPMs) are used to collect data for most beam-based optics characterization techniques used in emittance tuning at CesrTA. CESR is instrumented with 100 button-style peak-detection BPMs, with electronics developed in-house and capable of bunch-by-bunch, turn-by-turn readout for bunch spacings of $\geq 4\ \text{ns}$ [4]. A cross-section of a typical CESR BPM is shown in Fig. 3. At each BPM, all four button channels are read out by separate controller cards, therefore channel-to-channel crosstalk is minimized. Bunch-to-bunch cross-talk is below 4% after 4ns, and is effectively zero after 50ns; there is no turn-to-turn cross-talk. Shot-to-shot single-turn orbit reproducibility is approximately $10\ \mu\text{m}$. The BPM system has a buffer of approximately 300,000 bunch-turns. Depending on the user's request for data, some level of pre-processing is done on-board the BPM electronics before committing data to file, or the raw bunch-by-bunch turn-by-turn button signals are written directly to file.

The primary forms of BPM data used in optics correction are closed orbit, betatron phase and coupling, and dispersion. Turn-by-turn trajectory data is also used for BPM calibrations.

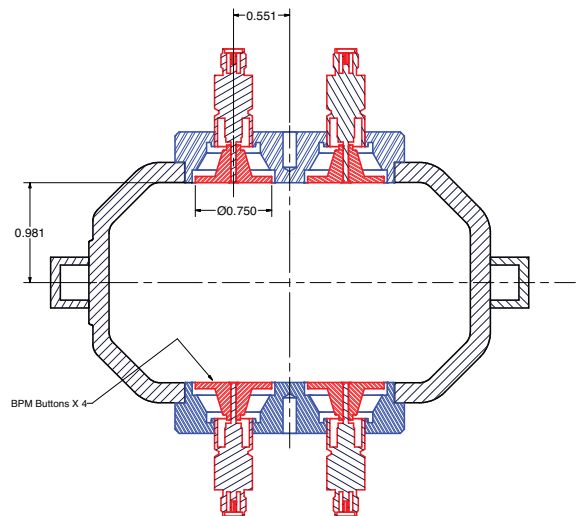


FIG. 3. Cross-section of a CESR BPM. Dimensions are in inches.

The closed orbit at each BPM is measured by aver-

aging 1024 turns of turn-by-turn bunch trajectory data onboard the BPM modules. A closed orbit measurement takes roughly 5 seconds, with measurement reproducibility of around $10\ \mu\text{m}$.

Quadrupole focusing errors are determined by measuring betatron phase advance, using turn-by-turn data acquired while resonantly exciting the beam [5]. Resonant excitation is achieved through a pair of “tune trackers,” which are stripline kickers phase-locked to the horizontal and vertical betatron tunes [6]. The tune trackers excite the beam to amplitudes of several millimeters. Phase and amplitude data are extracted from 40,960 consecutive turns by a processor onboard the BPM module for each button. The button-by-button phase and amplitude are post-processed into horizontal and vertical phase, the out-of-phase component of the coupling matrix \tilde{C}_{12} , and the two in-phase components of the coupling matrix $\tilde{C}_{22,11}$. All of the above information is processed from one measurement of the machine. Betatron phase and coupling measurements take roughly 10 seconds per measurement. Reproducibility of betatron phase measurements is of order 0.1 deg.

Dispersion measurements are performed by varying the RF frequency by a known amount, which changes the beam energy, and measuring the closed orbit. This is a direct measurement of the dispersive trajectory, and is well-understood and straightforward to execute. A standard dispersion measurement at CESR varies the 500 MHz superconducting RF cavities by $\pm 2\ \text{kHz}$ (corresponding to $\delta_E/E = 5.9 \times 10^{-4}$) and takes several minutes to acquire. Most of the required time is due to varying the RF frequency. The measurement reproducibility is better than 1 mm.

IV. BPM CALIBRATIONS

In order to ensure that measurements reflect actual machine conditions, BPMs must be well-calibrated. The primary characteristics to consider are: button-by-button timing, button-to-button relative gains, BPM tilts, and BPM-to-quadrupole transverse offsets.

Many modern lightsource BPMs take four signals into one controller that pre-processes the raw signals into horizontal and vertical data. CESR BPMs have four separate controller cards, one for each button, which read out independently. This allows for greater flexibility in measurements and post-processing, however some characteristics such as timing and gains must be calibrated on each of the four button channels rather than once per BPM.

Each of the required calibrations are now discussed in the order of implementation.

A. BPM Timing

Each controller card has independent timing, therefore every button on every BPM must be timed in separately. A mistimed channel results in sampling the bunch passage off-peak, which reduces the observed signal amplitude for that button.

The time-in procedure consists of sampling the temporal profile of a bunch passage at a resolution of 10 ps and fitting to determine the peak. The process takes less than one minute for all four buttons on all 100 BPMs to converge, with less than 10 ps drift over a period of four hours.

B. Button-to-Button Relative Gains

Differential response of the four BPM buttons due to variations in relative electronic gain will introduce a systematic measurement error. Measurements that depend mostly on position, such as orbit, dispersion, and the in-phase components of the coupling matrix $\tilde{C}_{22,11}$, are sensitive to relative button gains. Measurements using relative phase, such as betatron phase advance and the out-of-phase coupling matrix element \tilde{C}_{12} are largely insensitive to gain errors.

The method of gain mapping used at CEsrTA was developed by Rubin *et al.* at Cornell [7], and is based on a second-order expansion of the button signal response. The method utilizes turn-by-turn data, therefore data acquisition is fast, on the order of several seconds to collect data for characterizing all 100 BPMs.

The analysis relies on the fact that a linear relation exists between two combinations of the four button signals. For n turns of turn-by-turn trajectory data there are $4n$ button measurements at each BPM. There are only four unknowns, namely the button gains, and the system is overconstrained for $n > 1$ orbits; typically 1024 turns are used. Data acquisition takes about 10 seconds, and the fitting process takes less than a minute to determine all four button gains on all 100 BPMs.

All gain calibration techniques for peak-detection-style BPMs are sensitive to timing errors. This method is insensitive to detector rotation or offset, as the method uses raw button signals across a large cross-section of the BPM, and does not rely on distinguishing between horizontal and vertical modes.

Typical BPM gain variations before correction are of order 5%, and are calibrated with a reproducibility of a few tenths of a percent.

C. BPM Electronic Centering

A relative offset between the electronic center of a BPM and the magnetic center of the nearest quadrupole will appear in measurements as an offset in the quad. If the relative offset is not calibrated, steering the beam

to the electronic center of the BPM will result in kicks from the quadrupole, generating dispersion. To minimize vertical dispersion (and thus the emittance) generated during orbit correction, the relative offset between the electronic center of a BPM and the magnetic center of the nearest quadrupole must be measured.

BPM-to-quadrupole centering is achieved using resonant excitation data [8]. For each BPM/quadrupole pair, two consecutive betatron phase measurements are taken, with two different quadrupole settings. The difference in phase measurements is fit to determine the actual change in quadrupole strength, so that there is no reliance on a current-to-field calibration, which may be unreliable due to hysteresis.

The closed orbit is measured simultaneously with each phase measurement, and is therefore known before and after the change in quadrupole strength. The difference in closed orbits is fit to determine the kick induced by the quadrupole. The relative offset is then determined from the change in kick to the beam due to the change in strength of the quadrupole. The beam is then shifted toward the center of the quadrupole to improve the accuracy of the measurement, and the calibration is repeated.

BPM-to-quadrupole relative centering will only affect orbit measurements and turn-by-turn trajectory data. Dispersion measurements are a difference of two closed orbits, therefore absolute offsets do not affect the measurement. Betatron phase and coupling measurements are computed button-by-button, therefore transverse offsets will not affect the measurement.

Typical BPM-to-quadrupole offset measurements are around 1mm RMS in both horizontal and vertical, with a reproducibility of 170 μm .

D. BPM Tilt Calibration

If a BPM is rotated, a horizontal orbit perturbation will indicate a vertical offset. This becomes particularly significant when measuring the dispersion, as the average horizontal dispersion in CESR is large, on the order of a meter. A 10 mrad BPM tilt will couple a 1m horizontal dispersion into an apparent 10 mm vertical dispersion, which would then distort optics corrections. Simulations have shown that an RMS of 10 mm of actual vertical dispersion corresponds to 15 – 30 pm vertical emittance.

As previously mentioned, when acquiring betatron phase and coupling data, three of the four elements of the \bar{C} matrix are measured. For coupling corrections only the out-of-phase component \bar{C}_{12} is used, which is insensitive to BPM tilts. When the machine is well-corrected (i.e., \bar{C}_{12} is small), the residual in-phase components $\bar{C}_{22,11}$ will be dominated by BPM tilt errors; the in-phase components can therefore be fit to derive the BPM tilts, which can then be utilized when processing dispersion data.

Simulations of this method of BPM tilt calibration suggest that even when including effects of finite mea-

surement resolution and BPM measurement errors the method can determine BPM tilts to within 2.5 mrad. Measurements of the vertical dispersion suggest that the distribution of BPM tilts has an RMS of around 12 mrad or less. BPM tilt corrections will be implemented during the next dedicated CEsrTA machine studies period.

V. BEAMSIZE INSTRUMENTATION - XBSM

The primary method of determining the effectiveness of vertical emittance tuning is direct observation of the vertical beam size, from which the emittance can be inferred. CESR is instrumented with two x-ray beam size monitors (xBSM), one for each species [9, 10].

The xBSMs are one-dimensional 32-diode arrays with 50 μm pixel pitch. The instruments are capable of bunch-by-bunch, turn-by-turn measurements with a buffer of 250,000 bunch-turns. Dynamic range for the instruments span beam currents 0.25 – 10 mA = 0.4 – 16 $\times 10^{10}$ /bunch at the standard CEsrTA operating energy of 2.085GeV.

When characterizing low-emittance conditions, the beam is typically imaged using a horizontal slit, which acts as a one-dimensional pinhole. In practice, the resolution limit when using the pinhole optics is around 10 – 15 μm . The vertical beta function β_y at the xBSM source point is 40 m, and the xBSM optics provide a magnification of approximately 2.2. Therefore, the xBSMs are able to resolve the vertical emittance down to 2.5 – 5.5 pm. Beam size is determined by fitting to the beam profile over 1024 turns on a turn-by-turn basis, then averaging. In this way any effect of turn-by-turn centroid motion is removed from the measured beam size.

VI. LOW-EMITTANCE TUNING

The low-emittance tuning procedure developed at CEsrTA takes advantage of the fact that all magnets are independently powered, and all BPMs are capable of betatron phase and coupling measurements through turn-by-turn acquisition. The procedure is as follows:

1. Measure the closed orbit and correct to a reference orbit (which aligns the beam with the xBSM beamline) using all 55 horizontal and 58 vertical steering correctors.
2. Measure the betatron phase, transverse coupling (\bar{C}_{12}), and horizontal dispersion. Fit the model lattice to the measurement using all 100 quadrupoles and 27 skew quadrupole correctors, and load the computed corrections.
3. Remeasure the closed orbit, transverse coupling, and vertical dispersion. Fit the model lattice to all machine data simultaneously using all vertical steerings and skew quadrupoles, and load the fitted corrector changes.

The turnaround time for one full set of corrections is roughly ten minutes. It is standard procedure when first recovering conditions to save magnet settings after achieving low emittance, run the machine through a well-defined hysteresis loop, re-load the previously saved conditions, and repeat the emittance tuning procedure to apply minor corrections and ensure the desired conditions are reproducible.

Lattice corrections are determined by a χ^2 minimization where a machine model is fit to measurements of the lattice functions, with a merit function defined as [5]:

$$\chi^2 = \sum_i w_i^{data} [d^{measured}(i) - d^{model}(i)]^2 + \sum_j w_j^{var} [v^{measured}(i) - v^{model}(i)]^2 \quad (1)$$

where $d(i)$ is the i^{th} datum (for example, the vertical orbit at a BPM), $v(j)$ is the j^{th} variable (such as a corrector strength), and $w_{i,j}$ are user-defined weights. The merit function is minimized by adjusting corrector magnets in the model such that the model reproduces the measurements. The negative of the machine model corrector strengths are then loaded into the machine to compensate for optics errors.

Beam-based characterization of the machine after a typical low-emittance correction is shown in Table II. The discrepancy between the model that best fits those measurements and the design demonstrates the effectiveness of the correction.

TABLE II. Typical levels of correction for optics measurement after the full emittance tuning procedure. Measurements were taken at 0.8 mA (1.3×10^{10} /bunch), and RMS values are reported for both the machine measurement and a machine model which is fit to the measurements. Beta beat is computed from fitting phase data.

Measurement	RMS (Data)	RMS (Model)	Units
δy	253	110	[μm]
$\delta\phi_{a,b}$	0.3	0.3	[deg]
$\delta\beta/\beta$	—	0.73%	[%]
η_y	13	5	[mm]
C_{12}	0.004	0.003	[-]

The emittance is determined from the beam size:

$$\epsilon_y = \frac{\sigma_y^2 - (\eta_y \frac{\sigma_E}{E})^2}{\beta_y} \quad (2)$$

where the beam size at the source point σ_y is calculated from the measured image at the xBSM σ_{im} , accounting for the magnification and finite pinhole size, and η_y , β_y are measured. Coupling is measured to be small and does not contribute significantly to the measured vertical beam size.

Statistical and systematic errors associated with measurements of vertical emittance with the xBSM are outlined in [11], and include contributions from: turn-by-turn beamsize fitting uncertainty; turn-by-turn beamsize fluctuation; uncertainty in pinhole size; uncertainty in β functions; uncertainty in longitudinal location of the x-ray source point; and uncertainty in dispersion at the source point. The uncertainties propagate as follows:

$$\delta\epsilon_y^{sys} = \left| \frac{d\epsilon_y}{d\sigma_{im}} \right| \delta\sigma_{im}^{sys} + \left| \frac{d\epsilon_y}{d\sigma_p} \right| \delta\sigma_p + \left| \frac{d\epsilon_y}{ds} \right| \delta s \quad (3)$$

$$\delta\epsilon_y^{stat} = \left(\left| \frac{\partial\epsilon_y}{\partial\beta_y} \right|^2 (\delta\beta_y^{stat})^2 + \left| \frac{\partial\epsilon_y}{\partial\eta_y} \right|^2 (\delta\eta_y^{stat})^2 + \left| \frac{\partial\epsilon_y}{\partial\sigma_{im}} \right|^2 (\delta\sigma_{im}^{stat})^2 \right)^{1/2} \quad (4)$$

where

$$\left| \frac{d\epsilon_y}{ds} \right| = \left| \frac{\partial\epsilon_y}{\partial\beta_y} \frac{\partial\beta_y}{\partial s} + \frac{\partial\epsilon_y}{\partial\eta_y} \frac{\partial\eta_y}{\partial s} + \frac{\partial\epsilon_y}{\partial M} \frac{\partial M}{\partial s} \right| \quad (5)$$

and *sys* and *stat* refer to the systematic and statistical uncertainties, respectively. The individual terms $d\epsilon_y/dx_i$ are computed by varying the terms x_i in the emittance calculation by their uncertainties $\pm\delta x_i$. Relevant parameters used in the calculation of the emittance and the propagation of uncertainties are summarized in Table VI. Note that for the magnification M and optics functions β , η , the systematic uncertainties are accounted for through $\partial x_i/\partial s$ to emphasize their sole dependence on longitudinal source point in the dipole.

TABLE III. Parameters and uncertainties used for calculating uncertainty in beamsize measurement.

Parameter	Value	Sys.	Stat.	Units
σ_{im}	56.4	± 2.2	± 0.1	[μm]
σ_p	17.0	± 2.0	—	[μm]
M	2.1629	—	—	[-]
$\partial M/\partial s$	-0.4673	—	—	[m^{-1}]
β_y	42.09	—	± 0.75	[m]
$\partial\beta_y/\partial s$	-9.56	—	—	[m/m]
η_y	-0.9	—	± 2.0	[mm]
$\partial\eta_y/\partial s$	0.51	—	—	[mm/m]
δs	—	± 8	± 2	[mm]
σ_E/E	8.125×10^{-4}	—	—	[-]

Using the above tuning method, and propagating errors according to Equations 4–5, the vertical emittances achieved at CsrTA are reported in Table IV.

Several alternative LET tuning methods have been explored, including Orbit Response Matrix (ORM) analysis [12] and normal-mode analysis [13]. To date, no method has proven to be faster or yield consistently better results than the three-stage correction algorithm based on betatron phase and coupling measurements discussed here.

TABLE IV. Lowest-achieved emittance at CEsrTA in a variety of energies. Electron conditions are only reported for the April 2013 CEsrTA run at 2.085 GeV.

Energy [GeV]	Species	ϵ_y [pm]	$\delta\epsilon_y^{\text{sys}}$ [pm]	$\delta\epsilon_y^{\text{stat}}$ [pm]
2.085 (12/2012)	e^+	8.7	+2.9	+0.2
			-3.4	-0.2
2.085 (03/2013)	e^+	11.8	+3.3	+0.3
			-3.5	-0.2
2.085 (03/2013)	e^-	13.3	+3.4	+0.3
			-3.5	-0.3
2.305 (12/2012)	e^+	12.7	+3.0	+0.2
			-3.9	-0.2
2.553 (03/2013)	e^+	10.2	+2.9	+0.2
			-3.4	-0.2

VII. LET SIMULATIONS

To better characterize what factors are limiting emittance corrections, software has been developed to evaluate the contributions of misalignments, BPM measurement errors, and choice of correction procedure. The program, `ring_ma2`, uses the `Bmad` accelerator code library [14], and does the following:

1. Assigns random misalignments and BPM errors with user-defined amplitudes to the ideal lattice to create a realistic machine model.
2. Simulates beam based measurements of optics functions including the effects of BPM measurement errors.
3. Computes and applies corrections for each iteration based on the simulated measurements.
4. After each correction iteration, it records the effectiveness of the correction in terms of emittances and optics functions.

The entire procedure is repeated typically 100 times in order to generate statistics for analysis. The simulation is approached from a statistical perspective for three reasons. First, magnet positions continually drift, making it difficult to know the exact set of misalignments in the ring on any given day. Second, the precise distributions of magnetic centering or BPM measurement errors are not known, mandating that their distributions be approached from a statistical perspective. Third, by framing the analysis in terms of statistical probability of achieving the required emittance, the characterization process may be extrapolated to new machines which are not yet built using only the knowledge of survey and alignment tolerances.

When discussing the results of statistical analysis the 95% confidence levels (CL) are presented. That is, after applying the full optics correction procedure 95% of simulated lattices, each with a randomly chosen distribution of misalignments and measurement errors, achieve a

vertical emittance below the 95%CL. The simulation is believed to be sufficiently complete such that it is very unlikely that the contribution of the static optics to the vertical emittance is greater than this number.

In this section the method for simulating optics measurements is discussed, including how BPM measurement errors and guide field magnet errors are modeled. Results of simulations based on input parameters representing the physical accelerator are given.

A. Model Lattice with Errors

`Bmad` allows for introducing strength errors (including systematic and random multipole errors) and alignment errors (such as offset, roll, and pitch) to any lattice element. Magnet strength errors scale with the absolute strength of the magnet. Alignment errors are treated as additive errors, and are applied directly without scaling.

`ring_ma2` also models BPM measurement errors, which are discussed in detail in Section VII C.

B. Simulated Measurements

All simulated measurements are modeled as realistically as possible. For closed orbit measurements this involves recording 1024 turns of trajectory data, including the effects of BPM measurement errors on every turn, and averaging the results. Dispersion is simulated as a difference of two closed orbits, varying the RF frequency in-between.

For phase and coupling measurements, a particle is resonantly excited using a simulated phase-locked tune tracker and allowed to equilibrate by tracking for several damping times (10^5 turns). After the particle trajectory has equilibrated, 40,960 turns of raw BPM button data are recorded at every BPM. The data is then processed with the same code used for processing CESR phase and coupling data.

A comparison of lattice parameters derived from simulated measurements in an ideal lattice and those computed directly are summarized in Table V for each measurement type, and presumably represent a fundamental lower limit to the resolution of each measurement technique given no errors in the BPM measurements. Simulated measurements have differing levels of agreement for horizontal and vertical, which can be attributed to the aspect ratio of the BPM geometry and due to stochastic radiation emission in regions with horizontal dispersion.

C. BPM Errors

To generate simulated measurements as realistically as possible, BPM measurement errors must be taken into account. The two classes of BPM errors modeled in `ring_ma2` are BPM misalignments (offsets, tilts, and

TABLE V. RMS difference between simulated measurements and Bmad-calculated values, neglecting any BPM measurement errors.

Measurement	RMS (Simulated - Bmad)	Units
Closed Orbit x, y	$20, < 1 \times 10^{-3}$	[μm]
$\eta_{x,y}$	$0.75, < 1 \times 10^{-6}$	[mm]
$\phi_{x,y}$	0.1, 0.05	[deg]
\tilde{C}_{12}	4.3×10^{-4}	[-]

shear) and button-by-button effects (button gain, timing, and electronic noise). Each class of errors will affect the measurement differently. All simulated measurements presented include the effects of all listed BPM measurement errors.

1. BPM Misalignments

Errors in BPM misalignments (offsets and tilts) are applied in the following way:

$$\begin{pmatrix} x \\ y \end{pmatrix}^m = R(\theta) \begin{pmatrix} x^{lab} - \delta x \\ y^{lab} - \delta y \end{pmatrix} \quad (6)$$

where $(x, y)^m$ are the coordinates with BPM misalignments applied, $R(\theta)$ is the rotation matrix for angle θ , and $\delta x, \delta y$ are the horizontal and vertical offset between the BPM and nearest quadrupole.

2. Button Effects: Gain, Timing, and Reproducibility

Timing errors, gain variations, and turn-by-turn resolution affect individual button signals. Modeling their effects requires an accurate method for converting from (x, y) coordinates to button signals $b_{1,2,3,4}$, applying errors, and converting back to (x, y) coordinates.

All button-by-button errors of these classes are handled through use of a nonlinear interpolation grid which converts (x, y) coordinates to button signals. Button-by-button errors are applied to the individual channels, and the final “measured” (x, y) coordinates are determined by the best fit to the set of new button signals using the same interpolation grid [15]. The nonlinear map used in these studies is for a BPM with a “CESR geometry” (see Fig. 3).

Including effects from button-to-button gain errors, timing errors, and measurement reproducibility, the four observed button signals b_i at each BPM are:

$$b_i^{meas} = g_i t_i b_i^m + \delta b_i^{noise} \quad (7)$$

In Equation 7 b_i^m is defined to be the button signals determined through the interpolation grid for the coordinates $(x, y)^m$ from Equation 6. g_i is the gain error on

button i , and t_i is an effective gain error for button i arising from the timing error:

$$t_i = 1 - \frac{a_0}{a_2 + \frac{a_1^2}{4a_0}} (\delta t[s])^2 \quad (8)$$

where the constants $a_{0,1,2}$ are empirically determined. Note that because CESR BPMs are timed to the peak signal of a bunch passage, any timing error will decrease the button signal. This method of modeling the timing error also allows the BPM model to account for synchrotron motion, thus modulating the timings on all four buttons on a turn-by-turn basis.

BPM position measurement reproducibility is dominated by electronic noise arising from the digitization and amplification of an analog signal on each of the four controllers, and is modeled in Equation 7 as an additive error δb_i^{noise} on each of the four button signals. The amplitude of the button-by-button reproducibility is set by determining the change in a single button signal consistent with changing the observed orbit by the desired reproducibility (for example $10\mu\text{m}$).

Although actually a geometry error, relative shearing between the top and bottom BPM button blocks must be determined on a button-by-button basis, as it affects the top and bottom buttons differently. Upper and lower button signals are determined by offsetting the BPM in opposite directions.

D. Simulation Results

Amplitudes for misalignments and BPM errors in the simulation are summarized in Tables IX, X, and XI, and are determined either from directly-measured values or inferred from machine measurements. Offsets of quadrupoles and sextupoles include measured alignment levels along with $100\mu\text{m}$ added in quadrature to account for the estimated uncertainty in the offset of magnetic center with respect to geometric center of these elements.

The emittance correction procedure used in the simulation is identical to that used on the actual machine, outlined in Section VI. Results from `ring_ma2` are shown in Fig. 4, and summarized in Table VI.

TABLE VI. 95% confidence level (CL) correction levels after each correction iteration. All values except η_y^{Bmad} include observational effects from BPM measurement errors. Details of the correction iterations are discussed in Section VI.

Measurement	Initial	Iter 1	Iter 2	Iter 3	Units
ϕ	7.7	1.6	0.1	0.1	[deg]
η_y^{Meas}	42.6	18.7	18.7	15.4	[mm]
η_y^{Bmad}	40.1	13.9	12.2	5.0	[mm]
\tilde{C}_{12}	6.3	3.2	0.34	0.24	[$\times 10^{-2}$]
ϵ_y	255.8	33.0	27.5	4.1	[pm]

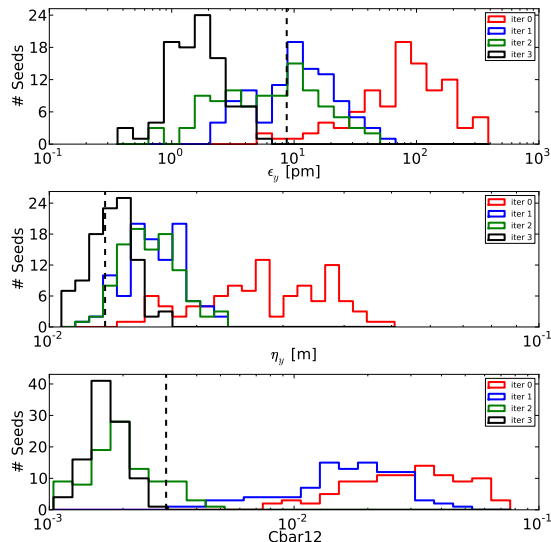


FIG. 4. Results from `ring_ma2`, using misalignments, BPM measurement errors, and multipoles stated in Tables IX, XI, and X, plotted before correction (red), and after first, second, and third stage of emittance correction (blue, green, and black, respectively). The dashed black line indicates typical measured values in CESR after low-emittance correction.

VIII. DIAGNOSIS OF EMITTANCE DILUTION

The measured vertical dispersion in Table II and the minimum \bar{C}_{12} measured at CEsrTA (2×10^{-3}) are within the distributions from the simulation. Increasing the coupling in simulated lattices such that the \bar{C}_{12} RMS is consistent with the measurement in Tab. II introduces a trivial amount of vertical emittance, less than 1 pm.

95% of the misaligned and corrected lattices from `ring_ma2` achieved vertical emittance below 4.1 pm, compared to the minimum measured vertical emittance of 8.7 (+2.9/-3.4) *sys* (± 0.2) *stat* pm at 2.085 GeV. It is unlikely that the discrepancy between measurement and the `ring_ma2` result is due to emittance measurement errors. This suggests that the emittance is not limited by anything modeled in the `ring_ma2` simulations, including magnet misalignment, field errors, multipoles, and correction method.

Possible candidates for the discrepancy include: time-varying sources of emittance dilution, such as magnet power supply and line voltage stability; contributions from the RF system; and collective effects.

A. Time-Varying Sources

Kicks which vary on a turn-by-turn basis will introduce emittance dilution. This has been directly observed in CESR, where the feedback modulators output a noise signal even when the modulator gain is set to zero. After amplification, this noise signal was sufficient to increase

the vertical emittance by 6.4 pm over the low-emittance measurement of 8.7 pm, an increase of more than 70%. Other time-varying sources of emittance dilution may be responsible for the remaining discrepancy between the measured emittance and `ring_ma2` simulation results.

Contributions to the vertical emittance from quantum excitation, magnet misalignments and field errors, and from time-varying sources each scale differently with energy. By measuring the minimum vertical emittance achieved at multiple energies, some understanding of their relative contributions may be gained.

The emittance is modeled as having four components, summing linearly:

$$\begin{aligned} \epsilon_b(E_0) &= \epsilon_b^{OA}(E_0) + \epsilon_b^{QE}(E_0) \\ &\quad + \epsilon_b^{RF}(E_0) + \epsilon_b^{\theta_c}(E_0) \\ &= C^{OA} F^{OA}(E_0) + C^{QE} F^{QE}(E_0) \\ &\quad + C^{RF} F^{RF}(E_0) + C^{\theta} F^{\theta}(E_0) \end{aligned} \quad (9)$$

$$(10)$$

where the four terms arise from the finite opening angle of the radiation fan, quantum excitation for radiation emission in dispersive regions, RF jitter, and time-varying dipole kicks. Wiggler contributions to the vertical emittance will scale differently than dipole contributions, as the wiggler field is held constant at all energies. As 90% of the synchrotron radiation is produced by the damping wigglers at CEsrTA, this will introduce a further energy dependence of the emittance, and has been accounted for in the analytic model.

The constants C^i denote the relative strength of the contributions, and are constrained to be positive. The energy-dependent functions $F^i(E_0)$ are normalized such that $F^i(2.085 \text{ GeV}) = 1$ and the constants C_i directly reflect the emittance contribution of each term, in picometers, at 2.085 GeV.

The emittance from the finite opening angle of the radiation fan (ϵ_b^{OA}) contributes minimally to the emittance (0.22 pm at 2.085 GeV), and scales minimally with energy (down to 0.18 pm at 2.553 GeV). This term is therefore fixed at 0.2 pm for these studies, to reduce the number of free parameters.

The vertical emittance was measured after corrections at 2.305 GeV and 2.553 GeV, in addition to the nominal 2.085 GeV. For all three energies the optics are constrained such that the differences are minimal, aside from B_{max} in the damping wigglers remaining at a fixed 1.9 T. Using measurements from Table IV, the constants C_i are determined through least-squares minimization.

Two scenarios are considered: first, assuming no contributions from RF jitter or time-varying dipole kicks, i.e., $C_{RF, \theta_s} = C_{\theta_c} = 0$; and second, allowing for both RF jitter and time-varying kicks. The resulting curves for emittance as a function of energy are shown in Fig. 5. The constants C_i for each scenario are summarized in Table VII.

It is not possible to distinguish between the two functions over the energy reach of CESR without further im-

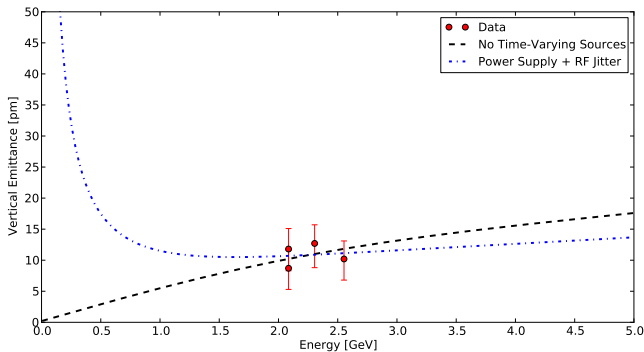


FIG. 5. Vertical emittance for a single bunch of positrons, as a function of energy. Measurements are shown in red, and were taken in December 2012 (2.085 GeV, 2.305 GeV) and April 2013 (2.085 GeV, 2.553 GeV). Two functional fits to the data are shown (black and blue dashed curves), using the form of Eqn. 10. Plotted error bars are systematic only, and indicate that all measurements would move in the same direction; statistical error bars are smaller than the data markers.

TABLE VII. Constants C_i for the three models of the energy dependence of the vertical emittance. Note that the functions $F^I(E_0)$ are normalized to be unity at $E_0 = 2.085$ GeV, therefore the constants C_i may be read as the contribution to the vertical emittance from that term at 2.085 GeV.

Scenario	C^{OA}	C^{QE}	C^{RF}	C^{θ_c}
No Jitter	0.2	10.016	0	0
Magnet, RF Jitter	0.2	7.29406	3.29793×10^{-5}	3.2025

improvements in the systematic uncertainties of the xBSM beam size measurements. Below 1.5 GeV the curves begin to diverge, however CESR has not been run below 1.5 GeV, and it is doubtful that the xBSM would have sufficient photon flux at such low energy to provide useful beamsizes measurements.

It is unlikely that no time-varying sources of emittance dilution exist in CESR, therefore the first scenario is unrealistic. When time-varying sources are allowed, the coefficient for RF jitter is negligible. This suggests that RF voltage jitter (and time-varying dipole kicks which scale inversely with energy) are not a significant source of emittance dilution. The coefficients also suggest approximately 3 pm of the vertical emittance at 2.085 GeV may be due to time-varying dipole kicks.

Although time-varying sources may potentially contribute 1/3 of the residual vertical emittance, it is still insufficient to bring the measurements into agreement with the `ring_ma2` simulation.

B. Emittance Dilution from RF

Turn-by-turn beam size was recorded while varying the total RF voltage and number of RF cavities powered. The results are summarized in Table VIII. It should be

noted that the studies summarized in this section were taken while one of the two West RF cavities was disabled, therefore only three RF cavities were used (one in the West, and two in the East). Nominal total RF voltage was 4.8 MV, distributed approximately evenly among the three cavities.

TABLE VIII. Summary of beam stability tests at CEsrTA. The measurements were conducted in April 2013, for a single bunch of positrons at 0.7-0.85 mA.

Total RF [MV]	East RF	West RF	ϵ_y [pm]
4.8	On	On	11.5
1.7	On	On	11.2
1.7	Off	On	12.5
1.7	On	Off	10.8

A small reduction in beam size was observed when reducing the total RF voltage from 4.8 MV to 1.7 MV, corresponding to a reduction in observed vertical emittance of 0.3 pm. The 1σ statistical uncertainty for the lowest-measured emittance is ± 0.2 pm. Note that although the systematic uncertainty is an order of magnitude larger, it represents a global uncertainty where all measurements would be affected uniformly by any change in the understanding of the beamsizes measurement system.

A further reduction is seen when the single West RF cavity is powered down and detuned, such that only the two East RF cavities are running; the emittance increased slightly when running only on the W1 RF cavity. This indicates that the RF system is contributing to the vertical emittance, although the extent or mechanism is not known at this time. The East and West RF cavity pairs run on separate power supplies; one hypothesis is that the West RF power supply is less stable than the East, thereby introducing vertical emittance through modulation of the RF voltage. Alternatively, by running a single cavity at a higher voltage, the amplitude of voltage jitter is also increased, potentially increasing the contribution to the emittance. The RF system in CESR is superconducting, therefore a direct examination of the alignment requires the nontrivial process of warming the cavities and opening the cryostats.

C. Collective Effects

The CEsrTA emittance target of 10 pm is for a “zero-current” beam; that is, neglecting any collective effects. It is possible, though unlikely, that the emittance at 0.8mA/bunch (1.3×10^{10} /bunch) is already diluted due to collective effects.

It is unlikely that electron cloud or fast-ion instability are contributing to the vertical emittance. Typically a train of 30 bunches with 0.5 mA/bunch or more is required in order for the emittance dilution from either of these effects to become visible, and the emittance blow-up takes place around bunch 10-15 in the train [16].

Extensive measurements and simulations on intra-beam scattering (IBS) at CEsrTA indicate that the vertical emittance is largely insensitive to IBS effects at currents $I < 1$ mA/bunch, where the measurements reported here were taken [17, 18]. The mechanism through which IBS increases vertical emittance depends on either transverse-to-longitudinal scattering in regions with dispersion or transverse-to-transverse scattering in regions with coupling, such that the vertical-mode action of the particle changes. Vertical dispersion and coupling are measured to be globally well-corrected, and are well below levels required for IBS to contribute to vertical emittance dilution.

By measuring beam size measurements at very low current, it may be possible to determine whether collective effects are contributing to the emittance at the nominal 0.8 mA/bunch used for the emittance measurements presented in Tab. IV. However, at such low current, photons are sparse and the turn-by-turn fitting procedure is no longer reliable. Instead, the turn-by-turn images must be averaged first in order to improve signal-to-noise, then fit as a single image. This has the disadvantages of incorporating a small amount of turn-by-turn beam motion and increasing the statistical uncertainty in the vertical emittance measurement.

Figure 6 shows the emittance calculated from a series of vertical beam size measurements from the xBSM, taken sequentially as the current was decreased from 1.1 mA to around 0.05 mA, and processed as described above.

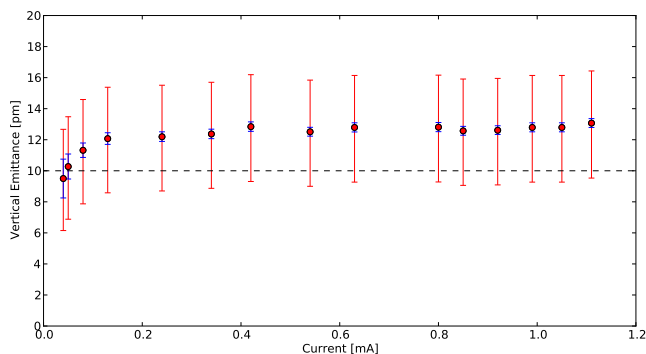


FIG. 6. Vertical emittance for a single bunch of positrons as a function of bunch current, from April 2013 CEsrTA machine studies. Plotted error bars are systematic (red) and statistical (blue). The dashed horizontal line indicates the 10 pm zero-current vertical emittance target for CEsrTA.

It is unclear whether the behavior at very low current (below 0.1 mA) is due to insufficient photon statistics for the xBSM analysis, or whether it is due to actual beam physics. As such, it is not possible to eliminate some form of collective effect with a very low-current threshold as a possibility. However, no known collective effect would display this current dependence, and the effect would have the unusual characteristic of saturating at very low

bunch current (below 1 mA = 1.6×10^{10} /bunch).

IX. CONCLUSIONS

A low-emittance tuning procedure has been developed at CEsrTA, based on betatron phase and coupling measurements using resonant excitation and turn-by-turn capable BPM. The tuning procedure has a fast turnaround, where one round of optics correction takes about ten minutes, and has yielded a single-bunch vertical emittance of $\epsilon_y = 8.7 (+2.9/-3.4)^{sys} (\pm 0.2)^{stat}$ pm with a single bunch of 0.8 mA = $1.3 \times 10^{10} e^+$ at 2.085 GeV. The correction procedure routinely achieves $\epsilon_y < 15$ pm in a variety of machine conditions at energies ranging from 2.085-2.5 GeV.

The energy dependence of the minimum-achieved vertical emittance suggests the vertical emittance continues to be dominated by contributions unaffected by optics correction, such as magnet power supply jitter. This is consistent with simulations suggesting that the contribution to vertical emittance from static optics errors is of order 3 pm or less. Although unlikely, collective effects have not been eliminated as a candidate for the observed emittance dilution. Further studies on sources of emittance dilution are scheduled for the next dedicated CEsrTA machine studies period.

Although misalignments do not appear to be the most significant contribution to the emittance, any improvement in alignment or optics correction will likely result in a small reduction in the emittance, as contributions add linearly. BPM tilts remain an outstanding issue. Alternative BPM tilt fitting techniques are under development. BPM tilt corrections will be implemented in the next dedicated machine studies period.

ACKNOWLEDGMENTS

The authors wish to thank the CESR operations and instrumentation groups, whose support was indispensable in our efforts to achieve well-corrected conditions. This work was supported by the National Science Foundation grant PHY-1002467 and the Department of Energy grant de-sc0006505.

Appendix: Errors for ring_ma2 Simulations

Table IX shows the misalignments and errors used in CEsrTA ring_ma2 studies. Offsets of quadrupoles and sextupoles include measured alignment levels along with $100 \mu\text{m}$ added in quadrature to account for the estimated uncertainty in the offset of magnetic center with respect to geometric center of these elements.

Systematic multipoles are included for sextupoles which have vertical steering or skew quadrupole trim windings. These multipoles are computed using field

modeling software, and are scaled to a measurement radius of 20 mm. There is a known random skew quadrupole component to the damping wiggler fields [19], due to manufacturing tolerances in the radii of the pole windings, which is also included. Multipoles used in this study are summarized in Table X.

TABLE IX. Misalignments and errors introduced into model CEsrTA lattice for `ring_ma2` studies. All parameters are determined either from machine measurements or survey.

Element Class	Error	RMS	Units
Dipole	x Offset	0.9	[mm]
	y Offset	2.0	[mm]
	s Offset	2.3	[mm]
	Roll	144	[μ rad]
	x Pitch	600	[μ rad]
	y Pitch	300	[μ rad]
Quadrupole	x Offset	350	[μ m]
	y Offset	107.8	[μ m]
	s Offset	5.2	[mm]
	Tilt	148	[μ rad]
	x Pitch	1100	[μ rad]
	y Pitch	62	[μ rad]
	k1	0.1%	[%]
Sextupole	x Offset	300	[μ m]
	y Offset	300	[μ m]
	s Offset	5.2	[mm]
	Tilt	200	[μ rad]
	x Pitch	1200	[μ rad]
	y Pitch	800	[μ rad]
	k2	0.1%	[%]
Wiggler	x Offset	1	[mm]
	y Offset	250	[μ m]
	s Offset	500	[μ m]
	Tilt	300	[μ rad]
	x Pitch	200	[μ rad]
	y Pitch	250	[μ rad]

TABLE X. Multipoles used in `ring_ma2` studies of CEsrTA lattice. Sextupole multipoles are systematic and therefore identical at all sextupoles, whereas the wiggler $a1$ multipole is random; the number quoted for wiggler $a1$ is therefore the RMS of the applied distribution.

Element Class	Multipole	Value
Sextupole with Vert. Steering Trim	a3	-7.25×10^{-4}
	a5	-1.46×10^{-2}
	a7	6.68×10^{-4}
	a9	8.7×10^{-6}
	a11	1.0×10^{-5}
Sextupole with Skew Quad Trim	a4	-1.2145×10^{-1}
	a6	2.16×10^{-4}
	a8	4.96×10^{-4}
	a10	-2.29×10^{-5}
	a12	-1.0×10^{-5}
Wiggler	a1	2.88×10^{-4}

TABLE XI. BPM errors introduced into model CEsrTA lattice for `ring_ma2` studies.

Error	Applied RMS	Units
Reproducibility	10	[μ m]
Tilt	12	[mrad]
Gains	0.5%	[%]
Timing	10	[ps]
Offset (x, y)	170	[μ m]
Horizontal Shear	± 100	[μ m]

-
- [1] M. A. Palmer *et al.*, in *Proceedings of the 2009 Particle Accelerator Conference, Vancouver, BC* (2009) pp. 4200–4204.
- [2] G. F. Dugan, M. A. Palmer, and D. L. Rubin, in *ICFA Beam Dynamics Newsletter*, No. 50, edited by J. Urakawa (International Committee on Future Accelerators, 2009) pp. 11–33.
- [3] D. Rubin, D. Sagan, and J. Shanks, in *Proceedings of the 2009 Particle Accelerator Conference, Vancouver, BC* (2009) pp. 2751–2753.
- [4] M. A. Palmer *et al.*, in *Proceedings of the 2010 International Particle Accelerator Conference, Kyoto, Japan* (2010) pp. 1191–1193.
- [5] D. Sagan, R. Meller, R. Littauer, and D. Rubin, *Phys. Rev. ST Accel. Beams* **3**, 092801 (2000), 10.1103/PhysRevSTAB.3.092801.
- [6] R. E. Meller and M. A. Palmer, in *Proceedings of the 2011 Particle Accelerator Conference, New York, NY* (2011) pp. 504–506.
- [7] D. L. Rubin *et al.*, *Phys. Rev. ST Accel. Beams* **13**, 092802 (2010), 10.1103/PhysRevSTAB.13.092802.
- [8] J. P. Shanks, D. Rubin, and D. Sagan, in *Proceedings of the 2010 International Particle Accelerator Conference, Kyoto, Japan* (2010) pp. 4620–4622.
- [9] N. T. Rider, J. P. Alexander, J. A. Dobbins, M. G. Billing, R. E. Meller, M. A. Palmer, D. P. Peterson, C. R. Strohmman, and J. W. Flanagan, in *Proceedings of the 2011 Particle Accelerator Conference, New York, NY* (2011) pp. 687–689.
- [10] N. T. Rider *et al.*, in *Proceedings of IBIC 2012: International Beam Instrumentation Conference, Tsukuba, Japan*, Paper WECD01 (in press).
- [11] J. Shanks *et al.*, in *Proceedings of the 2011 Particle Accelerator Conference, New York, NY* (2011) pp. 1540–1542.
- [12] J. P. Shanks *et al.*, in *Proceedings of the 2009 Particle Accelerator Conference, Vancouver, BC* (2009) pp. 2754–2756.
- [13] A. Wolski, D. Rubin, D. Sagan, and J. Shanks, *Phys. Rev. ST Accel. Beams* **14**, 072804 (2011), 10.1103/PhysRevSTAB.14.072804.
- [14] D. Sagan, *Nucl. Instrum. Methods Phys. Res.* **A558**, 356 (2006).
- [15] R. W. Helms and G. H. Hoffstaetter, *Phys. Rev. ST Accel. Beams* **8**, 062802 (2005), 10.1103/PhysRevSTAB.8.062802.
- [16] M. Billing *et al.*, in *Proceedings of the 2013 International Particle Accelerator Conference*.
- [17] M. Ehrlichman, *Normal Mode Analysis of Single Bunch, Charge Density Dependent Behavior in Electron/Positron Beams*, Ph.D. thesis, Cornell University, Ithaca, New York (2013).
- [18] M. P. Ehrlichman *et al.*, in *Proceedings of the 2012 International Particle Accelerator Conference, New Orleans, LA* (2012) pp. 2970–2972.
- [19] J. A. Crittenden, A. Mikhailichenko, E. Smith, K. Smolenski, and A. Temnykh, in *Proceedings of the 2005 Particle Accelerator Conference, Knoxville, TN* (2005) pp. 2336–2338.